Appl. Phys. B 62, 45–50 (1996)

Applied Physics B Lasers and Optics

Experimental evaluation of entropy for transmission holographic optical elements

L. Carretero[1], A. Beléndez[2], A. Fimia[1]

[1] Laboratorio de Optica, Departamento Interuniversitario de Optica, Universidad de Alicante, Apdo. No. 99, E-03080 Alicante, Spain (Fax: + 34-6/590-3464, E-mail: CARRETE@vm.cpd.ua.es)
[2] Departamento de Ingeniería de Sistemas y Comunicaciones, Universidad de Alicante, Apdo. No. 99, E-03080 Alicante, Spain

Received: 28 December 1994/Accepted: 12 April 1995

Abstract. An experimental study of transmission holographic optical elements is presented. Several important aspects related to the diffractional analysis of these elements have been considered. The case of the spherical object wave is analyzed in detail. The emphasis is on obtaining the entropy from the intensity distribution on an image plane. We use the calculated entropy to locate experimentally the position of the best image plane in the sense of minimal aberrations for a holographic lens. The comparison of experimental and theoretical results is presented and good agreement between theory and experimentation has been obtained.

PACS: 42.40.Dp; 42.40.Fr

An evaluation of the imaging quality of classical or holographic optical systems is possible by using the diffraction theory of aberrations [1–5]. The diffraction image given by an optical system from a point is known as the Point Spread Function (PSF), and this optical response function can be calculated from the design data [6]. This is still of great use to study the performance of an optical system with aberrations. By using this theory, it is possible to calculate the light intensity distribution on the image plane directly. In the previous papers, we used the diffraction theory to address a series of questions including intensity distribution in an image plane and its characterization through a series of statistical moments [7] and the axial irradiance [8] of a Holographic Optical Element (HOE) in the presence of spherical aberration. Recently, the concept of entropy has been used to locate the position of the best image plane for a HOE in the presence not only of small but also large aberrations [9]. In this paper, we are going to use an experimental optical setup to find out how all these theoretical results can be applied experimentally. We will begin with a detailed description of the experimental setup, and then we will present the most relevant results we obtained.

Let us outline the properties of hologram aberration derived by Champagne [10]. We assume that the HOE is located on the XY-plane, and the point source $Q(x_q, y_q, z_q)$ of a spherical wave is defined in terms of the parameters R_q, α_q, and β_q, as can be seen in Fig. 1. Here $q = \mathrm{r}, \mathrm{o}, \mathrm{c}$ and i denote the reference, object, reconstruction and image points, respectively. The recording and reconstruction wavelengths are λ_r and λ_c, respectively. The phase aberration Δ at a point (x, y) in the exit-pupil plane of the HOE is given by:

$$\Delta(x, y) = \phi_\mathrm{c}(x, y) - \phi_\mathrm{i}(x, y) \pm [\phi_\mathrm{o}(x, y) - \phi_\mathrm{r}(x, y)], \quad (1)$$

where ϕ_q is the phase of a spherical wave:

$$\phi_q(x, y) = \frac{2\pi}{\lambda_q}[r_q(x, y) - R_q]. \quad (2)$$

The phase aberration $\Delta(x, y)$ is related to the wave aberration $W(x, y)$ according to $\Delta(x, y) = (2\pi/\lambda_\mathrm{c})\, W(x, y)$. Using (1) and (2), $W(x, y)$ can be written as:

$$W = r_\mathrm{c} - r_\mathrm{i} \pm \mu(r_0 - r_\mathrm{r}) - [R_\mathrm{c} - R_\mathrm{i} \pm \mu(R_0 - R_\mathrm{r})], \quad (3)$$

where μ denotes the wavelength shift $\lambda_\mathrm{c}/\lambda_\mathrm{r}$. The geometry for calculating the diffraction patterns is shown in Fig. 2. We introduce a local coordinate frame $X'Y'Z'$ fixed to the Gaussian image point G as origin. The Z'-axis is defined by the principal ray which runs from the center of the hologram to the Gaussian image point and we choose the $X'Y'$-plane as the image plane, so that (x', y') are the coordinates of an image point H in this plane, while the coordinates of this image point in the XYZ coordinate system are $(x_\mathrm{i}, y_\mathrm{i}, z_\mathrm{i})$. The intensity of the image in a plane normal to the chief ray (the Z'-axis) at a distance z' from the center of the HOE may be written as [7] :

$$I(x', y'; z') = \frac{1}{B^2}\left|\iint_S A(x, y)\exp[\mathrm{i}\Delta(x, y; x', y', z')]\,\mathrm{d}x\,\mathrm{d}y\right|^2 \quad (4)$$

Part of this paper was presented at the IS & T/SPIE symposium in Electronic Imaging, Science and Technology (Practical Holography IX) February 4-10, 1995, San José, CA, USA

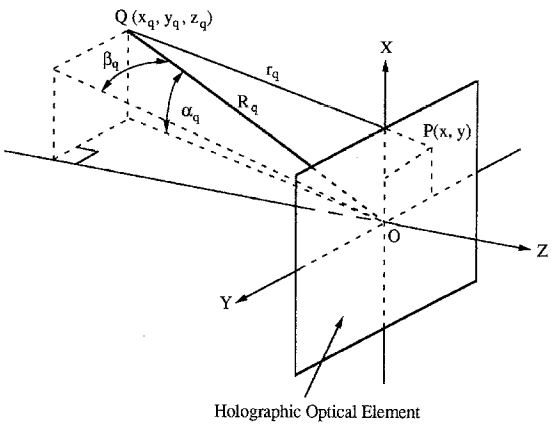

Fig. 1. Geometry used for the HOE analysis

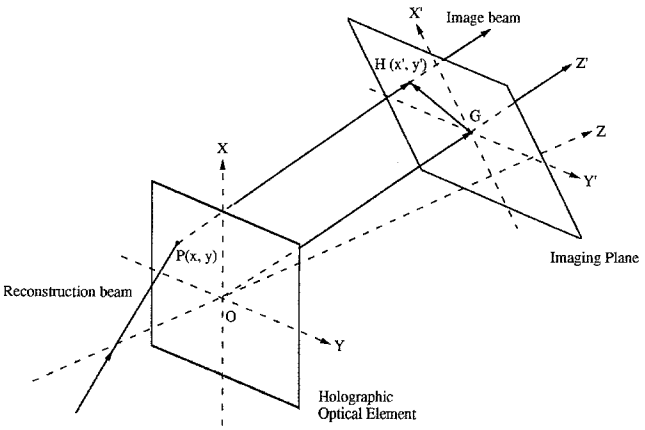

Fig. 2. Geometry used for calculating the diffraction patterns

for an uniform amplitude $A(x, y) = 1$ and S being the area of the exit pupil where the integration is done. In (4), B is the amplitude at the Gaussian image point ($x' = y' = 0$) in the absence of aberrations. Intensity can be interpreted as a probability density function, provided that it is adequately normalized as:

$$P(x', y'; z') = \frac{I(x', y'; z')}{\iint\limits_{A'} I(x', y'; z')\,dx'\,dy'}, \tag{5}$$

where A' is the integration area in the image plane. For an image plane situated at z' position, we can define the entropy of the image formed on this plane as [9] :

$$S(z') = -\iint\limits_{A'} P(x', y'; z') \ln[P(x', y'; z')]\,dx'\,dy', \tag{6}$$

and numerical calculations are necessary to obtain this entropy. In this case, entropy should be interpreted as a property of the way energy is distributed on an image plane intensity, and, in this sense, entropy gives us a measure of the aberrations in the considered plane. The lowest entropy plane will be the best image plane in the sense of minimal aberrations. In the presence of aberrations, this plane is different from the plane which contains the Gaussian image point.

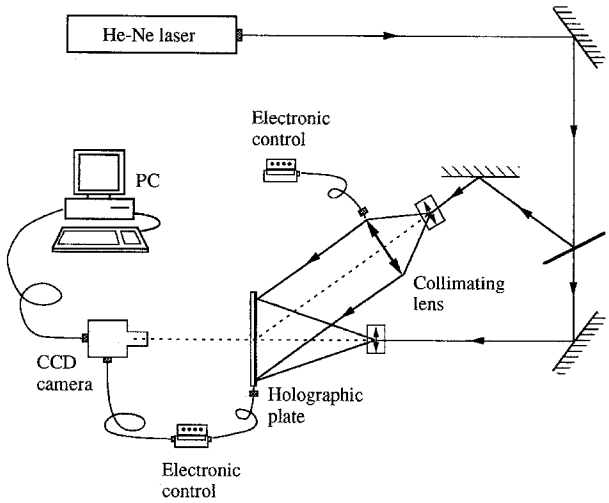

Fig. 3. Optical setup used to record holographic lenses

1 Experimental setup

An experimental setup was designed that allows for the diffraction analysis of HOEs recorded as off-axis elements. Figure 3 shows a simplified scheme of the setup. The laser beam is divided into two by a variable separating sheet. Using a 40X microscopic objective, one of the beams is expanded so that, by using a plano-convex lens, a beam is obtained whose degree of collimation can vary due to the fact that the lens is mounted on an electronically controlled micrometric axial translator that has a resolution of ± 0.1 μm. This will be both the reference beam during recording and the reconstruction beam. The second beam is expanded using a 40X microscopic objective which generates a divergent beam. This will be the object beam. The holographic plate is mounted on a rotating device which is also controlled electronically and which has a resolution of $\pm 0.001°$. Since this device is in turn situated on a micrometric precision stage, it is possible to obtain a very accurate repositioning of the HOEs.

In order to analyze the image beam coming from the HOE, we use a CCD camera mounted on XY mechanical micrometric translators, which in turn are mounted on an electrically controlled axial movement system with a sensitivity of ± 0.1 μm. With this camera, it is possible to obtain images that will be processed subsequently.

2 Experimental analysis of holographic lenses

Throughout the experimental study, several holographic lenses were manufactured and analyzed, each with a different recording and reconstruction geometry. One of them was chosen to be used as an example. The holographic lens that we selected was recorded through the interference of a spherical wave from a point source and a plane wave (Fig. 3) in Agfa 8E75 HD emulsion, using the 633 nm (λ_r) radiation of a He-Ne laser of 40 mW. The point source for the spherical wave was a pinhole measuring 25 μm in diameter. Spurious reflections were eliminated by placing an index-matched absorbing layer

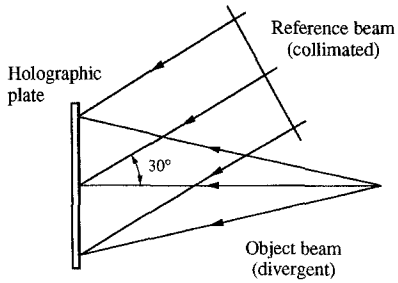

a

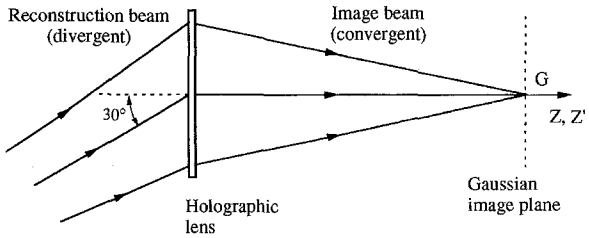

b

Fig. 4. **a** Recording and **b** reconstruction geometry of the analyzed lens

Table 1. Recording and reconstruction geometry parameters of the lens

$R_r = \infty$	$\alpha_r = 30°$	$\beta_r = 0°$
$R_0 = 40$ cm	$\alpha_0 = 0°$	$\beta_0 = 0°$
$R_c = -413$ cm	$\alpha_c = 0°$	$\beta_c = 0°$
$\lambda_r = 633$ nm	$D = 10.45$ mm	

against the glass side of the photographic plate. Polarization of the recording beams was perpendicular to the plane in Fig. 3, and the usable diameter of the lens was 10.45 mm. The object wave was an on-axis spherical wave, and the reference wave was a plane wave at an angle of 30°. The distance between the point source of the spherical wave and the center of the plate was 40 cm. We chose one of the recording waves as a plane wave in order to simplify both recording and reconstruction.

The exposure level used was 40 μJ/cm^2 with a beam ratio of ≈ 1. After exposure, the plate was developed in a PAACM developer, which consists of a solution of Phenidone (0.5 g), Ascorbic Acid (18 g), sodium Carbonate (120 g) and Methol (2 g) in 1 l of distilled water. After a brief rinse, the plate was bleached without a fixation step with an R-10 rehalogenating-type bleach. This bath was composed of potassium dichromate (2 g) , sulfuric acid (10 ml), and potassium bromide (35 g) diluted in 1 l of distilled water. This processing technique is known to introduce small changes in the emulsion thickness [11].

Once the lens was processed, the HOE was reconstructed using the setup described in the previous section with light from the same laser that was used in the recording stage ($\lambda_c = \lambda_r = 633$ nm). The lens was reconstructed with a -413 cm divergent beam that was obtained by modifying the position of the collimating lens shown in Fig. 3. Figure 4 shows a recording and reconstruction scheme for the holographic lens analyzed. During reconstruction, the lens is rotated 180° to obtain a convergent image wave. This is equivalent to considering that the recording was done with a collimated beam and a convergent beam. The parameters of the lens shown in Table 1 are used.

Using the recording geometry shown in Table 1, the aberration coefficients of the holographic lens are the following [10] :

Spherical abberration coefficient	$S = 4.10 \times 10^{-6}\,\mathrm{cm}^{-3}$
Comma coefficient	$C_x = 2.90 \times 10^{-6}\,\mathrm{cm}^{-2}$
Astigmatism coefficient	$A_x = -6.05 \times 10^{-4}\,\mathrm{cm}^{-1}$.

The maximum aberration-wave values for spherical aberration, comma, and astigmatism are 3.05×10^{-7}, 4.10×10^{-7}, and 1.60×10^{-4} cm, respectively. From these values, we obtain that the dominant aberration in the recorded holographic lens is astigmatism.

3 Calculating entropy

In order to calculate the entropy, experimental diffraction figures must first be obtained. Figure 5 shows the experimental setup that was used to obtain the entropy. Once the holographic lens is manufactured and respositioned, it is reconstructed as mentioned in Sect. 2.

On the optical axis of the lens, we find a CCD camera (Sony, XC-75CE) which is also mounted on a micropositioning device which allows the distribution of intensities to be captured in any image plane perpendicular to the optical axis. The camera gives us a high-resolution image with 752×582 pixels. Each pixel measures 8.6 μm × 8.4 μm (horizontal/vertical), and this allows us to calculate the real size of the image from the number of pixels on the computer screen. The CCD camera is connected to a computer with a Data Translation DT 3851 digitized card. The image is initially digitized with the software package known as GLOBAL LAB Image.

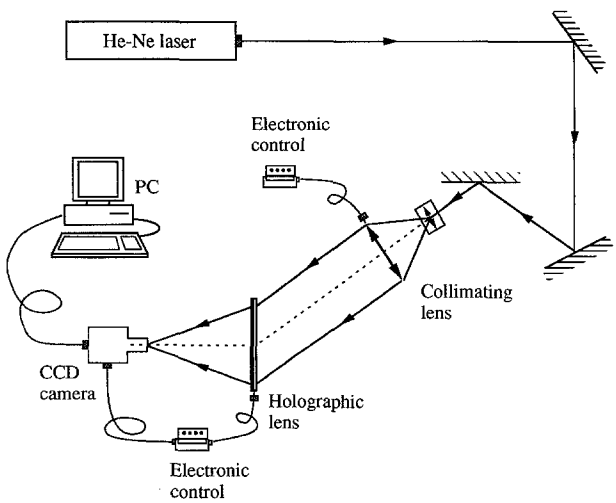

Fig. 5. Optical setup used to obtain entropy

Since theoretically, we work with a finite-size image plane, the size used in the experiment to analyze the image should be the same as the one used in the theoretical numerical calculations. In order to calculate entropy (and subsequently axial irradiance), a total of 22 images were captured. The position of the CCD camera was moved 0.1 cm between the images, covering a total distance along the optical axis of 2.2 cm.

In order to analyze the image, a file was generated which contained an M_{ij} squared matrix made up of whole numbers whose values indicated the gray level in the pixel placed at position (i, j) in relation to a system of Cartesian coordinates centered on the upper left vertex of the image. A software program has been developed (in Turbo Pascal) for data-processing purposes that makes it possible to calculate the entropy of each plane image from the M_{ij} matrix.

The first step is to normalize the M_{ij} matrix to one. This is done by dividing the value of the gray level stored by the maximum value possible, which in this case is 255. In other words:

$$M_{ij} \rightarrow W_{ij} = M_{ij}/255.$$

After normalizing the matrix, we can see that a background that is not zero exists which was not taken into account in the theoretical calculations and that this background is due to noise.

This background noise is not cummulative, and in general, its values are relatively low. One way to suppress it is to rescale the image so that $L_{ij} = W_{ij} - M_0$ for $W_{ij} > M_0$ and zero for other cases. The value of M_0 is determined by analyzing the image's histogram. This technique is valid when the signal-to-noise ratio is large. However, when we analyze planes in which the signal noise is low, we do not get good results. In the cases we analyzed, this happened when image planes in marginal zones were analyzed.

It is also possible to calculate the FFT of each image plane and to use a filter to eliminate the noise frequencies, thereby obtaining a definitive image through an inverse Fourier transform. However, we thought that this option would be too slow. The option that was used to eliminate the background noise R in each image plane consisted of calculating the average value $\langle R \rangle$ from the intensity found in a square in the dark zone of the image. Once the average noise was calculated, the W_{ij} matrix was rescaled so that

$$W_{ij} \rightarrow F_{ij} = \mathrm{Abs}(W_{ij} - \langle R \rangle),$$

where "Abs" indicates the absolute value of the magnitude which is used to make sure that $F_{ij} > 0$. With this new definition, we are using intensity values that are closer to the ones used in the theoretical calculations.

In order to calculate the entropy, it is necessary to work with the distribution of probability associated with each image plane. The total intensity T for each image that is captured is calculated using the following equation:

$$T = \sum_{i=1}^{N} \sum_{j=1}^{M} F_{ij}, \tag{7}$$

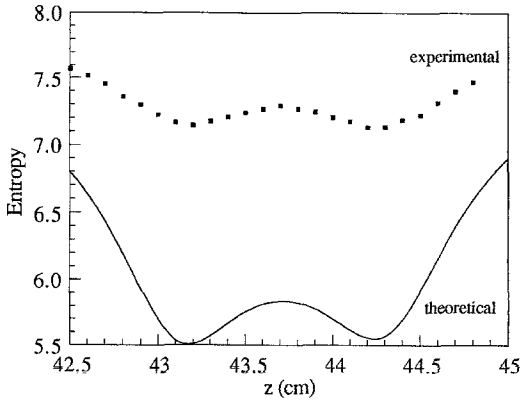

Fig. 6. Theoretical and experimental entropy with background noise

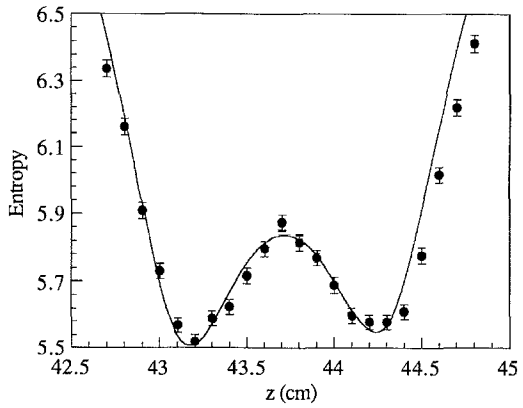

Fig. 7. Theoretical and experimental entropy without background noise

where $N \times M$ is the total number of pixels in the image. By using this value, we can define the discrete distribution of probability P_{ij} associated with the corresponding plane as:

$$P_{ij} = \frac{F_{ij}}{T}. \tag{8}$$

From this distribution, the entropy associated with the plane S can be numerically calculated by using the equation

$$S = -\sum_{i=1}^{N} \sum_{j=1}^{M} P_{ij} \ln P_{ij}. \tag{9}$$

Figure 6 shows the experimental entropy obtained when background noise is not taken into account and the theoetically calculated entropy for the holographic lens described in Sect. 2. As can be seen, the value of the experimental entropy is greater than the theoretical entropy obtained numerically. This is due to the fact that background noise implies that there is more disorder in the image plane, and an increase in the disorder in an image implies a greater value of the entropy. However, qualitatively, the shape of the two curves and the position of the minimum and maximum values coincide.

Figure 7 shows the entropy obtained experimentally when the intensity was corrected for background noise in

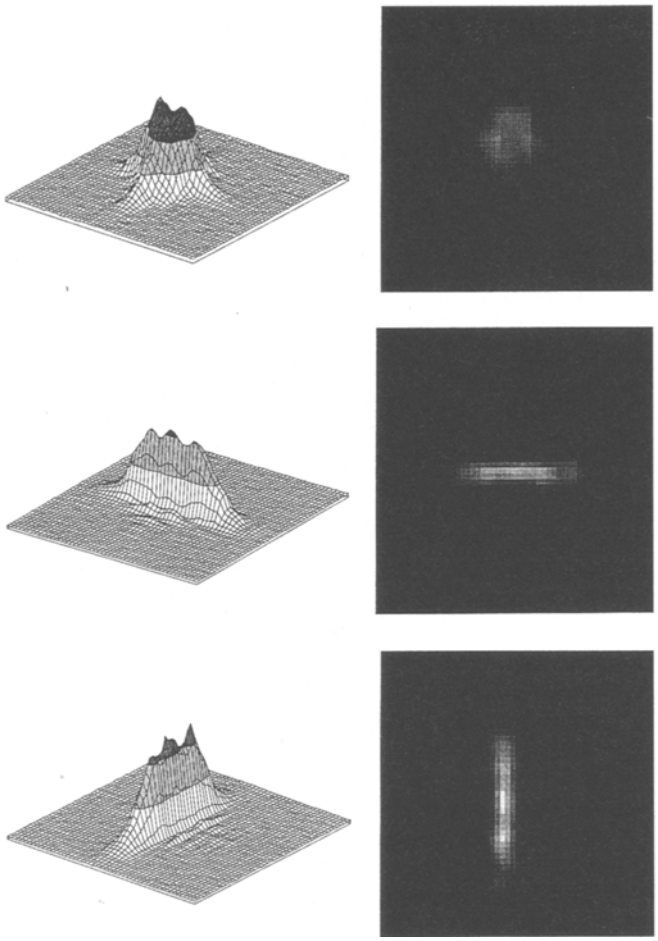

Fig. 8a–c. Experimental distribution of intensities obtained for (**a**) the relative maximum of the entropy, (**b**) the first minimum of the entropy, and (**c**) the second minimum of the entropy

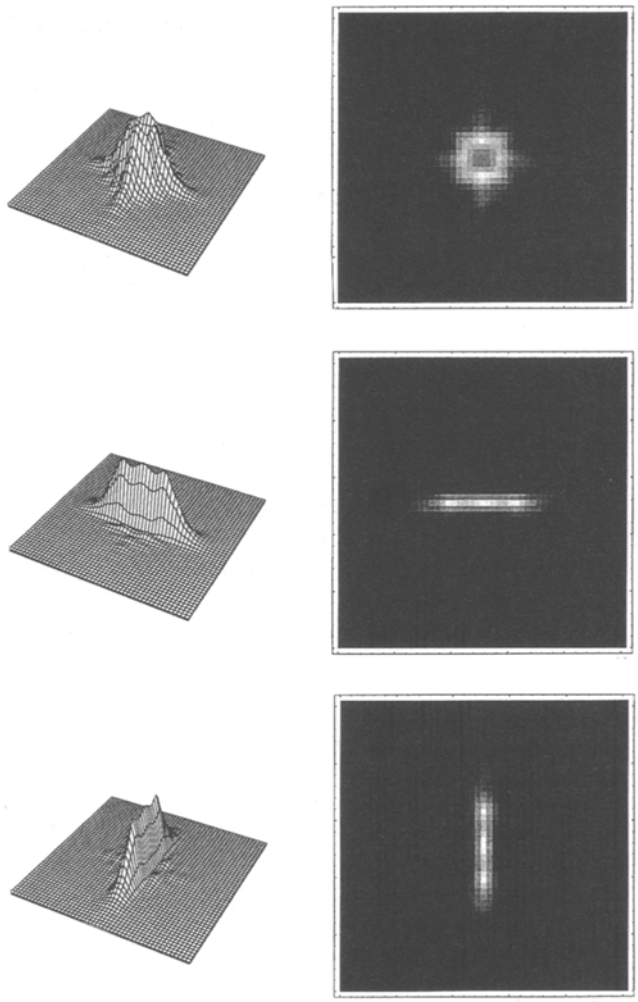

Fig. 9a–c. Theoretical distribution of intensities obtained for (**a**) the relative maximum of the entropy, (**b**) the first minimum of the entropy, and (**c**) the second minimum of the entropy

each plane, as was indicated earlier. As can be seen in this case, the curves coincide both qualitatively and quantitatively. This agreement makes it possible to state that the entropic function can be used to determine if the correct noise filter was used for the image. As was indicated in Sect. 2, the lens is essentially astigmatic when this recording and reconstruction geometry is used. Therefore, the lens has two Sturm focal points (Sturm's focals) and the circle of minimum astigmatic confusion is found exactly half way between these two focal points.

Figure 8 shows the experimental distributions of the intensity obtained using the CCD camera for the positions corresponding to the relative maximum and the two absolute minimums of the entropic function. This proves that they correspond to the minimum confusion circle and the two Sturm focal points. Figure 9 shows the same figures obtained theoretically using the numerical program that we developed.

4 Calculation of axial irradiance

The next step was to obtain the axial irradiance of the holographic lens shown in Fig. 4. To calculate the axial irradiance the M_{ij} matrix that was obtained experimentally was always used. Starting with the level of gray for each image plane, we found the corresponding central pixel. By appropriately normalizing the gray level, we can find the normalized axial irradiance value (Strehl ratio) for this plane. Figure 10 shows the axial irradiances obtained theoretically and experimentally. As we see, the agreement between the two is quite good. Therefore, this method makes it possible to obtain the axial irradiance quickly and more easily than by using other methods that have been proposed recently [12].

5 Conclusions

We performed an experimental study of a transmission HOE using Agfa 8E75 HD photographic emulsion and an R-10 rehalogenating bleach without a fixation step. The diffractional analysis of these elements was investigated and the entropy calculated from measurements of the light intensity distribution in the image plane. Using the values of the entropy, we have obtained the best imaging plane

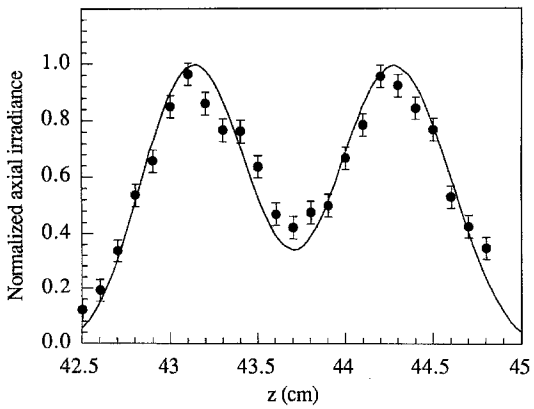

Fig. 10. Theoretical (*solid line*) and experimental axial irradiance

for an holographic lens whose dominant aberration is astigmatism. The analyses shown in this paper give us important evidence about the potential of the use of the entropy for the study of the imaging quality in holographic systems. Finally, the experimental study presented in this paper can also be extended to conventional optics.

Acknowledgements. We gratefully acknowledge the financial support of the Direcció General d'Ensenyaments Universitaris i Investigació (grant GV-1165/93), Generalitat Valenciana, Spain.

References

1. H.H. Hopkins, M.J. Yzuel: Opt. Acta **17**, 157 (1970)
2. J. Nowak, M. Zajac: Opt. Acta **30**, 1749 (1983)
3. C.S. Chung, H.H. Hopkins: J. Mod. Opt. **35**, 1485 (1988)
4. I. Banyasz, G. Kiss, P. Varga: Appl. Opt. **27**, 1293 (1988)
5. S. Baskar, K. Singh: J. Mod. Opt. **38**, 1517 (1991)
6. M. Born, E. Wolf: *Principles of Optics* (Pergamon, Oxford 1987)
7. L. Carretero, A. Fimia, A. Beléndez: J. Opt. **26** (1995) (in press)
8. A. Beléndez, L. Carretero, A. Fimia: Opt. Lett. **19**, 1477 (1994)
9. L. Carretero, A. Fimia, A. Beléndez: Opt. Lett. **19**, 1355 (1994)
10. E.B. Champagne: J. Opt. Soc. Am. **57**, 51 (1967)
11. L. Carretero, A. Beléndez, A. Fimia: J. Mod. Opt. **40**, 687 (1993)
12. Q. Gong, S. S. Hsu: Opt. Eng. **33**, 1176 (1994)